

Topological Spaser

Jih-Sheng Wu,^{*} Vadym Apalkov,[†] and Mark I. Stockman[‡]
Center for Nano-Optics (CeNO) and Department of Physics and Astronomy,
Georgia State University, Atlanta, Georgia 30303
 (Dated: October 8, 2019)

We theoretically introduce a topological spaser, which consists of a hexagonal array of plasmonic metal nanoshells containing an achiral gain medium in their cores. Such a spaser can generate two mutually time-reversed chiral surface plasmon modes in the \mathbf{K} - and \mathbf{K}' -valleys, which carry the opposite topological charges, ± 1 , and are described by a two-dimensional E' representation of the D_{3h} point symmetry group. Due to the mode competition, this spaser exhibits a bistability: only one of these two modes generates, which is a spontaneous symmetry breaking. Such a spaser can be used for an ultrafast all-optical memory and information processing

The concept of the surface plasmon amplification by stimulated emission of radiation (spaser, also called plasmonic nanolaser) [1–3] has recently been experiencing rapid development. Many different types of spasers have been proposed [4–7] and demonstrated [8–18]. The spasers were also applied to various problems including explosives detection [19], monitoring of the nano-environment [20, 21], cancer therapeutics and diagnostics (theranostics) [22].

A particular type of the spasers is represented by plasmonic crystals that include gain media [7, 13, 23, 24]. Such spasers belong to the class of lasing spasers [7], which are nanostructured plasmonic metasurfaces consisting of a periodic lattice of individual spasers. Due to interactions in the near-field, the individual spasers lock in phase to generate temporally- and spatially-coherent fields. However, such a fundamental question as the effects of topological properties (the Berry curvature) [25, 26] of the plasmonic Bloch bands of such crystals has not yet been investigated.

Recently, a groundbreaking work has been carried out aimed at obtaining a topological lasing in a plasmonic-photonic (diffractive) lattice of honeycomb symmetry [27]. The plasmonic lasing was observed at the \mathbf{K} -points but only in a mode of the A'_1 symmetry, which is a singlet (scalar) representation. Therefore, this mode does not possess a chiral topological charge.

In this Letter, we propose a topological spaser that geometrically is a deeply-subwavelength two-dimensional (2d) crystal (metasurface) with a honeycomb symmetry built of two different triangular sublattices, A and B – see Fig. 1. A metaatom of such a lattice is a plasmonic metal nanoshell containing an achiral gain medium, similar to the spaser geometry of Ref. 3. The A- and B-sublattices of such a topological spaser differ in size and shape of the constituent nanoshells (see the caption to Fig. 1), so their individual spasers have different eigenfrequencies. Note that a natural example of a honeycomb lattice consisting

of two different sublattices is provided by the transition metal dichalcogenide (TMDC) crystals [28–30].

The spasing eigenmodes are surface plasmons (SPs) that should be classified corresponding to irreducible representations of the symmetry point group of the lattice unit cell, which is D_{3h} [31]. This group has six representations, of which E' is a two-dimensional (doublet) representation with the desired properties – see Appendix. It describes two degenerate modes time-reversed to each other, which carry topological charges of $Q_T = \pm 1$ defining their chirality; their local fields rotate in time and space in the opposite directions.

For the proposed topological spaser, we will show that the degenerate eigenmodes at the \mathbf{K} - and \mathbf{K}' -points strongly compete with each other, making such a topological spaser bistable: either $Q_T = 1$ or $Q_T = -1$ mode can generate. These spasing modes are topological Berry plasmons [32]. However, in Ref. 32, the system's chirality was due to the induced valley polarization. In a sharp contrast, in our case the system is originally achiral and \mathcal{T} -reversible: no integral Berry curvature or magnetic field are present; the chirality is self-organized due to the mode competition causing a spontaneous violation of the \mathcal{T} -reversal and σ'_v -reflection symmetries.

The quasistatic SPs eigenmodes [33] are electric potentials, $\varphi_{\nu\mathbf{k}}(\mathbf{r})$, characterized by lattice momentum \mathbf{k} and band index ν . These eigenmodes can be found from the quasistatic equation [34]

$$\nabla [\Theta(\mathbf{r})\nabla\varphi_{\nu\mathbf{k}}(\mathbf{r})] = s_{\nu\mathbf{k}}\nabla^2\varphi_{\nu\mathbf{k}}(\mathbf{r}), \quad (1)$$

where $1 > s_{\nu\mathbf{k}} > 0$ are the eigenvalues, and $\Theta(\mathbf{r})$ is the characteristic function, which is 1 inside and 0 outside the metal. These eigenmodes satisfy an orthonormality condition: $\int \nabla\varphi_{\nu\mathbf{k}}\nabla\varphi_{\nu'\mathbf{k}'}^*d^3r = \delta_{\nu\nu'}\delta_{\mathbf{k}\mathbf{k}'}$.

We employ the tight-binding approximation where the on-site states are the modes of isolated metal nanoshells, and the coupling between them is the nearest-neighbor dipole interaction. For each nanoshell, we consider two eigenmodes constituting a basis for the E' doublet representation of the D_{3h} point symmetry group, $\varphi_m^{(\alpha)} \propto Y_{1m}$, where Y_{1m} are the spherical harmonics, $m = \pm 1$, and $\alpha = A$ or B. These eigenmodes with $m = \pm 1$ have the electric field components in the xy -plane of the lattice and are coupled by the dipole interaction.

^{*}Electronic address: b91202047@gmail.com

[†]Electronic address: vapalkov@gsu.edu

[‡]Electronic address: mstockman@gsu.edu

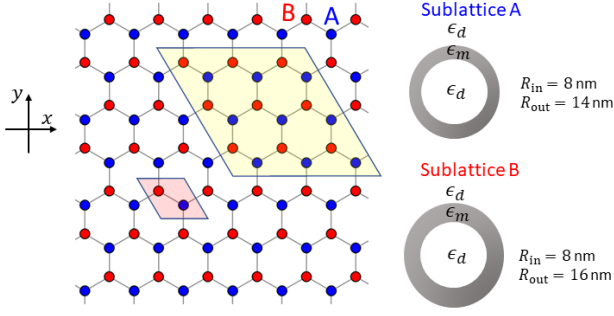


FIG. 1: Honeycomb array of metal nanoparticles. It consists of two inequivalent sublattices: A and B. Sublattice A consists of plasmonic metal nanoshells with the inner radius of 8 nm and the outer radius of 14 nm while sublattice B consists of similar nanoshells with the inner radius of 8 nm and the outer radius of 16 nm. The gain medium is placed inside the nanoshells. The lattice bond length is set as 50 nm. The primitive unit cell of the honeycomb crystal structure is shown by the red parallelogram. The supercell, which describes the periodicity of the SP's at both the \mathbf{K} - and \mathbf{K}' -points, is marked by the yellow parallelogram. (9)- (12), is marked by the yellow parallelogram.

The eigenmodes $\varphi_m^{(\alpha)}$ of an isolated nanoshell of a sublattice $\alpha = A, B$ satisfy the following equation [cf. Eq. (1)]

$$\nabla \left[\Theta^{(\alpha)}(\mathbf{r}) \nabla \varphi_m^{(\alpha)}(\mathbf{r}) \right] = s_m^{(\alpha)} \nabla^2 \varphi_m^{(\alpha)}(\mathbf{r}). \quad (2)$$

where $\Theta^{(\alpha)}(\mathbf{r})$ is 1 inside the metal of nanoshell α and 0 elsewhere, and \mathbf{r} is relative to the center of this nanoshell. The solution of Eq. (2) can be expressed as an expansion over the spherical harmonics, Y_{lm} , see Appendix.

With the known eigenmodes of the isolated nanoshells, we express the quasistatic potential for a mode with quantum numbers ν, \mathbf{k} as a sum over the lattice and $m = \pm 1$,

$$\varphi_{\nu\mathbf{k}}(\mathbf{r}) = \sum_{j\alpha m} C_{\nu\mathbf{k}m}^{(\alpha)} \sqrt{s_m^{(\alpha)}} \exp(i\mathbf{k}\mathbf{R}_j^{(\alpha)}) \varphi_m^{(\alpha)}(\mathbf{r} - \mathbf{R}_j^{(\alpha)}), \quad (3)$$

where $\mathbf{R}_j^{(\alpha)}$ is the lattice vector of the nanoshell j center in sublattice α . Expansion coefficients $C_{\nu\mathbf{k}m}^{(\alpha)}$ satisfy the following tight-binding equations

$$\sum_{\alpha'm'} H_{\alpha m, \alpha'm'}(\mathbf{k}) C_{\nu\mathbf{k}m'}^{(\alpha')} = s_{\nu\mathbf{k}} C_{\nu\mathbf{k}m}^{(\alpha)}. \quad (4)$$

Here the nearest neighbor tight-binding Hamiltonian is

$$H_{\alpha m, \alpha'm'} = \begin{cases} s_m^{(\alpha)} \delta_{mm'}, & \alpha = \alpha', \\ \sqrt{s_m^{(\alpha)}} \sqrt{s_{m'}^{(\alpha')}} \sum_{j'} \exp[i\mathbf{k}(\mathbf{R}_{j'}^{(\alpha)} - \mathbf{R}_j^{(\alpha)})] \times \\ \int \nabla \varphi_m^{(\alpha)*}(\mathbf{r} - \mathbf{R}_j^{(\alpha)}) \nabla \varphi_{m'}^{(\alpha')}(\mathbf{r} - \mathbf{R}_{j'}^{(\alpha')}) d^3r, & \alpha \neq \alpha', \end{cases} \quad (5)$$

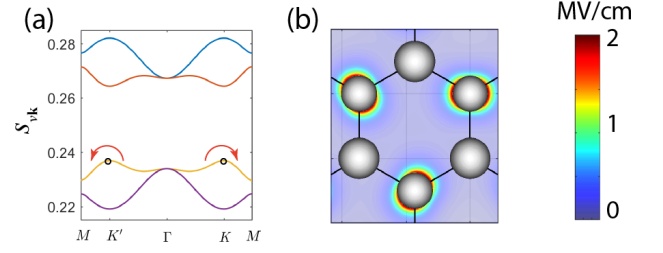


FIG. 2: (a) Band structure of the honeycomb array of metal nanoshells. Due to the broken inversion symmetry, i.e., sublattices A and B being inequivalent, there are band gaps at the \mathbf{K} - and \mathbf{K}' -points. The spasing SP modes at the \mathbf{K} - and \mathbf{K}' -points are indicated by open circles; the arrows indicate the direction of the rotation of the local modal fields for the corresponding valleys. (b) Profile of the electric field of an SP at the valence band in the \mathbf{K} -valley at a certain instance of time. Only the SPs at sublattice A are excited. The color bar to the right codes the modal field amplitude.

where j is an arbitrary lattice site, and j' are the nearest-neighbor sites to it.

The solution of Eq. (4) produces four bands whose dispersions are shown in Fig. 2(a). Due to the broken inversion symmetry owing to the sublattices A and B being inequivalent, there are band gaps opened at the \mathbf{K} - and \mathbf{K}' -points.

The structure of SP excitations at these points is the following. At either the \mathbf{K} -point or the \mathbf{K}' -point, the SP modes are excited in the real space only on a single sublattice, A – see an illustration in Fig. 2(b). The SPs at the \mathbf{K} - and \mathbf{K}' -points are mutually time-reversed: the magnetic quantum numbers are $m = \pm 1$ corresponding to the topological charges $Q_T = \pm 1$, and the phase shifts between the nearest sites on the A sublattice are $\pm 2\pi/3$, respectively, as illustrated in Fig. 3(a)-(d). Below we assume that the frequency of the optical transitions in the gain medium is equal to the frequency of SPs in the valence band at the \mathbf{K} - and \mathbf{K}' -points – see a schematic in Fig. 3(e).

The SP's at the \mathbf{K} - and \mathbf{K}' -points have equal frequencies, $\omega_{\nu\mathbf{K}} = \omega_{\nu\mathbf{K}'}$, as protected by the \mathcal{T} symmetry. We write down the Hamiltonian of the plasmonic system in the second quantization as

$$H_{SP} = \hbar\omega_{\nu\mathbf{K}} \left(\hat{a}_{\nu\mathbf{K}}^\dagger \hat{a}_{\nu\mathbf{K}} + \hat{a}_{\nu\mathbf{K}'}^\dagger \hat{a}_{\nu\mathbf{K}'} \right), \quad (6)$$

where $\hat{a}_{\nu\mathbf{k}}^\dagger$ and $\hat{a}_{\nu\mathbf{k}}$ are the SP creation and annihilation operators. Here the frequency $\omega_{\nu\mathbf{k}}$ is found from equation $\text{Re}[s(\omega_{\nu\mathbf{k}})] = s_{\nu\mathbf{k}}$, where $s(\omega) = \epsilon_d/(\epsilon_d - \epsilon_m(\omega))$ is the Bergman spectral parameter, ϵ_d and $\epsilon_m(\omega)$ are the dielectric functions of the host material and the metal, respectively. The corresponding electric field is given by [1]

$$\mathbf{E}(\mathbf{r}, t) = - \sum_{\mathbf{k}=\mathbf{K}, \mathbf{K}'} A_{\nu\mathbf{k}} \nabla \varphi_{\nu\mathbf{k}}(\mathbf{r}) (\hat{a}_{\nu\mathbf{k}} + \hat{a}_{\nu\mathbf{k}}^\dagger), \quad (7)$$

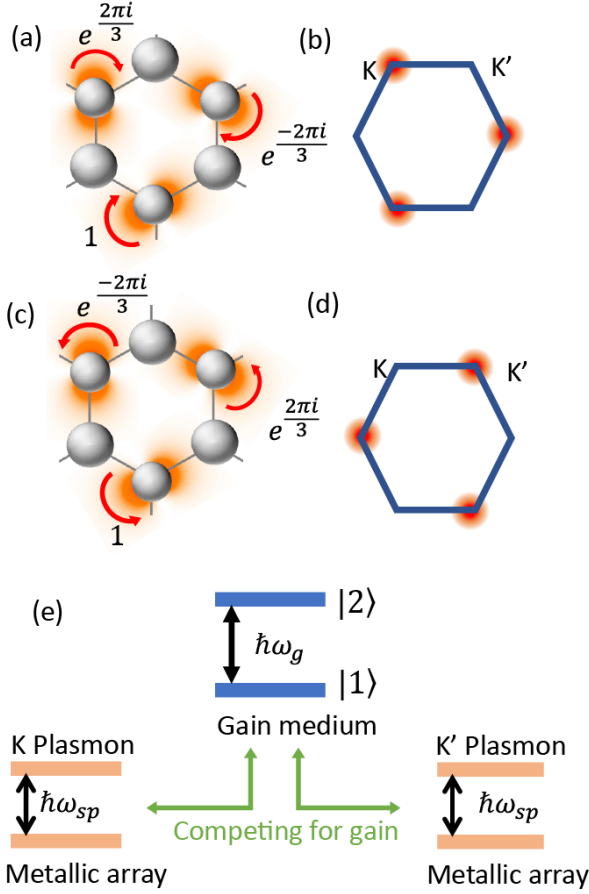


FIG. 3: (a)-(d) The valence band SPs in the \mathbf{K} - and \mathbf{K}' -valleys. For both the valleys, only the SPs at the sublattice A are excited. For the \mathbf{K} -valley, these are the SPs with $m = 1$, while for the \mathbf{K}' -valley, the SP with $m = -1$ are generated. Their phase shifts from site to site are $2\pi/3$ and $-2\pi/3$, respectively. The SP local fields rotate in the directions shown by the red arrows. (e) Schematic illustration of the system of gain medium and metal array. The SPs at the \mathbf{K} - and \mathbf{K}' -points compete for the same gain.

where $A_{\nu\mathbf{k}} = \sqrt{4\pi\hbar s_{\nu\mathbf{k}}/\epsilon_d s'_{\nu\mathbf{k}}}$, $s'_{\nu\mathbf{k}} = \text{Re}[ds(\omega)/d\omega|_{\omega=\omega_{\nu\mathbf{k}}}]$.

The gain medium is assumed to be achiral with a linear transition dipole moment \mathbf{d} ; this dipole equally couples to both the \mathbf{K} and \mathbf{K}' SP modes. The gain medium is described quantum mechanically using density matrix $\rho^{(p)}$ for a p th nanoshell. Within the rotating wave approximation (RWA), the non-diagonal elements of the density matrix can be written as $(\rho^{(p)})_{12} = \bar{\rho}^{(p)} \exp(i\omega_{\nu\mathbf{K}}t)$, while the diagonal elements determine the population inversion, $n^{(p)} = \rho_{22}^{(p)} - \rho_{11}^{(p)}$. The interaction between the gain medium and the SP system is determined by Hamiltonian

$$H_{int} = - \sum_p \mathbf{E}(\mathbf{r}^{(p)}, t) \mathbf{d}^{(p)}. \quad (8)$$

Following Ref. 3, we treat the plasmonic field quasi-

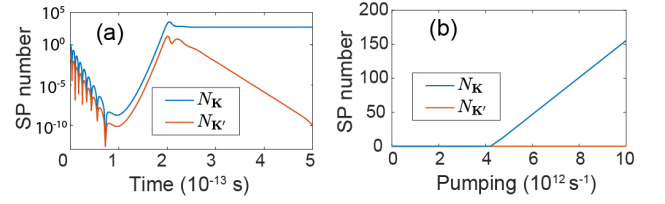


FIG. 4: Dynamics of SP population per unit supercell. (a) Temporal dynamics of the SP population. Initially the SPs in both the valleys are present, which is case (iii) – see the text. The pumping rate is $g = 10^{13} \text{ s}^{-1}$. (b) The stationary number of SPs in both valleys as a function of pumping rate.

classically by replacing the creation and annihilation operators of the SP's by the respective complex c -number amplitudes $a_{\nu\mathbf{K}}$, $a_{\nu\mathbf{K}'}$, and $a_{\nu\mathbf{K}}$, $a_{\nu\mathbf{K}'}$. The corresponding SP population numbers per the composite unit cell are $N_{\mathbf{K}} = |a_{\nu\mathbf{K}}|^2$ and $N_{\mathbf{K}'} = |a_{\nu\mathbf{K}'}|^2$.

The coupled system of equations [3], which describes both the SPs and the gain medium, takes the following form

$$\dot{a}_{\nu\mathbf{K}} = -\gamma_{sp} a_{\nu\mathbf{K}} + iN_g \sum_p \bar{\rho}^{(p)*} \tilde{\Omega}_{\nu\mathbf{K}}^{(p)*}, \quad (9)$$

$$\dot{a}_{\nu\mathbf{K}'} = -\gamma_{sp} a_{\nu\mathbf{K}'} + iN_g \sum_p \bar{\rho}^{(p)*} \tilde{\Omega}_{\nu\mathbf{K}'}^{(p)*}, \quad (10)$$

$$\dot{n}^{(p)} = -4\text{Im} \left[\bar{\rho}^{(p)} \sum_{\mathbf{k}=\mathbf{K},\mathbf{K}'} \tilde{\Omega}_{\nu\mathbf{k}}^{(p)} a_{\nu\mathbf{k}}^{(p)} \right] + g(1 - n^{(p)}) - \gamma_2(1 + n^{(p)}), \quad (11)$$

$$\dot{\bar{\rho}}^{(p)} = -\Gamma_{12} \bar{\rho}^{(p)} + i n^{(p)} \sum_{\mathbf{k}=\mathbf{K},\mathbf{K}'} \tilde{\Omega}_{\nu\mathbf{k}}^{(p)*} a_{\nu\mathbf{k}}^{(p)*}, \quad (12)$$

where N_g is the number of electrons of the gain medium inside each shell, γ_{sp} is the SP relaxation rate, γ_2 is the non-radiative decay rate of the level $|2\rangle$ of the chromophore, Γ_{12} is polarization relaxation rate for the $|2\rangle \rightarrow |1\rangle$ transition of the chromophores, g is the excitation (pumping) rate per a chromophore, and $\tilde{\Omega}_{\nu\mathbf{k}}^{(p)} = \frac{1}{\hbar} A_{\nu\mathbf{k}} \nabla \varphi_{\nu\mathbf{k}}(\mathbf{r}^{(p)}) \mathbf{d}^{(p)}$ is the Rabi frequency. In computations, we set: $\epsilon_d = 2$, $d = 10$ debye, $N_g = 514$, $\gamma_{sp} = 4.1 \times 10^{13} \text{ s}^{-1}$, $\Gamma_{12} = 2.1 \times 10^{14} \text{ s}^{-1}$, and $\gamma_2 = 4 \times 10^{12} \text{ s}^{-1}$. We used dielectric data [35] for silver as the nanoshells' metal.

The Rabi frequencies, $\tilde{\Omega}_{\nu\mathbf{K}}^{(p)}$ and $\tilde{\Omega}_{\nu\mathbf{K}'}^{(p)}$, are periodic with respect to the position vector, $\mathbf{r}^{(p)}$, with the periods that are determined by the crystal momenta \mathbf{K} and \mathbf{K}' , respectively. Any solution of Eqs. (9)-(12), which contains both the \mathbf{K} and \mathbf{K}' components, will be periodic on a superlattice with an eighteen-nanoshell unit cell (“super-cell”) shown in Fig. 1. Then the summation over p in Eqs. (9) and (10) is extended over the corresponding eighteen points.

As initial conditions for Eqs. (9)-(12), we set $n^{(p)}(t)|_{t=0} = -1$, which implies that initially all the chromophores of the gain medium are in the ground state.

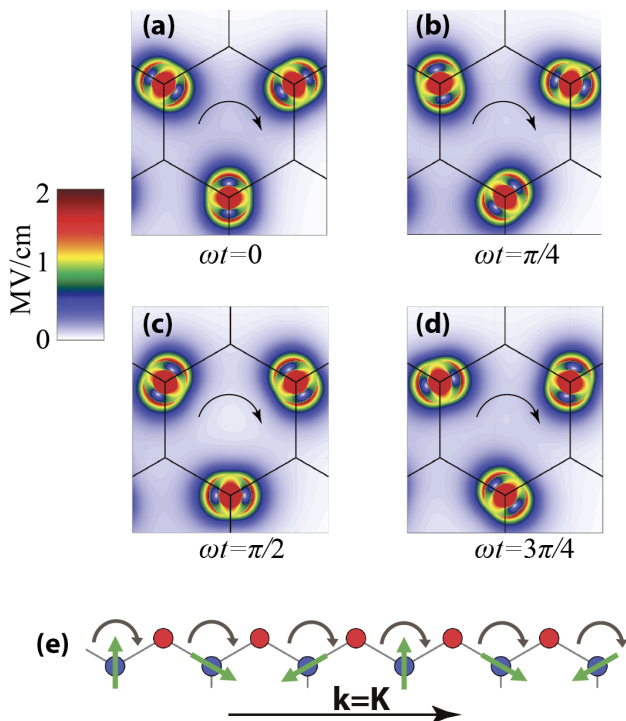


FIG. 5: Dynamics of \mathbf{K} -valley SP eigenmode. (a)-(d) The distributions of the local field modulus are plotted for the unit cell in the real space. The phases of the spaser oscillation are indicated for each panel. The color-coded scale of the local fields is given at the left-hand side for one SP quantum per the unit supercell. The local fields rotate in time in the direction of the black arrow, i.e., clockwise. (e) Edge fields for \mathbf{K} -valley mode. The instantaneous dipole vectors are indicated by the green arrows; the direction of the field rotation is depicted by the curved black arrows; crystal momentum \mathbf{k} of the mode is shown by the straight black arrow. Each such a rotating dipole generates a current that is normal to this dipole.

Similarly, we assume that initially there is no polarization, $\bar{\rho}(t)|_{t=0} = 0$. With respect to the initial SP amplitudes, $a_{\nu\mathbf{K}}$ and $a_{\nu\mathbf{K}'}$, we consider three cases: (i) The initial SP amplitude is small and located only at the \mathbf{K} -point where we set $a_{\nu\mathbf{K}} = 0.1$ and $a_{\nu\mathbf{K}'} = 0$; (ii) The same as the previous case but with the SP amplitude located at the \mathbf{K}' -point, $a_{\nu\mathbf{K}} = 0$ and $a_{\nu\mathbf{K}'} = 0.1$; (iii) The SP's are initially present at both the \mathbf{K} - and \mathbf{K}' -points but with different amplitudes, $a_{\nu\mathbf{K}} = 1$ and $a_{\nu\mathbf{K}'} = 0.2$.

We start with case (iii) where initially both the \mathbf{K} - and \mathbf{K}' -valleys are weakly populated, with a higher population at the \mathbf{K} -point, which emulates a random initial condition created by quantum fluctuations. The pumping begins at $t = 0$ with a rate of $g = 10^{13} \text{ s}^{-1}$. The dynamics of the SP populations in both the valleys as a function of time t after the beginning of the pumping is displayed in Fig. 4(a). As we see, after the initial period of decay and relaxation oscillations, the population of the dominant \mathbf{K} -valley starts growing exponentially and then levels off becoming stationary with the SP population $N_{\mathbf{K}} \approx 150$. At the same time, the minor SP population,

$N_{\mathbf{K}'}$, decays exponentially for $t \gtrsim 200$ fs. This occurs due to a strong competition of the \mathbf{K} - and \mathbf{K}' -modes for the common gain. At the same time, the decay to zero, $N_{\mathbf{K}'} \rightarrow 0$, implies that there is no cross-mode talk, which is due to the topological protection: these two SP modes carry conserved topological charges $Q_T = \pm 1$. Due to the \mathcal{T} -symmetry, the valleys are symmetric: starting with the \mathbf{K}' -valley with a dominant SP population, the final population will only be in that valley. Thus the topological spaser is a topologically-protected symmetric bistable device.

The kinetics of the topological spaser, i.e., the dependence of the stationary SP population numbers, $N_{\mathbf{K}}$ and $N_{\mathbf{K}'}$ for $t \rightarrow \infty$, as functions of the pumping rate g , is illustrated in Fig. 4(b) for case (i) when only the \mathbf{K} -valley has a non-zero initial population: $N_{\mathbf{K}} = 0.01$ and $N_{\mathbf{K}'} = 0$. There is a pronounced threshold after which the SP population in the \mathbf{K} -valley grows linearly with the pumping rate. The population in the \mathbf{K}' -valley remains zero due to the topological protection. Similarly, in case (ii), the SP population will be amplified and remain only in the \mathbf{K}' -valley.

The dynamics of the real-space distributions of the local fields in the topological spaser is shown in Fig. 6 (a)-(e) for the case of the \mathbf{K} -valley generation (see also Appendix for the \mathbf{K}' mode). The fields are normalized to one SP in the unit supercell. This distribution contains three dipolar fields localized on the A-sublattice nanoshells, which rotate clockwise in the optical cycle. This field distribution is generally chiral and compliant with the E' representation of the D_{3h} group. At a given moment of time, this field distribution can also be described as a chiral lattice wave propagating in the clockwise direction along the unit cell boundary. The 2d E' representation also describes a mode with the opposite (counter-clockwise) chirality, which can be obtained by an application of either \mathcal{T} or σ'_v symmetry operations.

The present topologically-charged E' spasing mode is indeed dark: obviously, it does not possess a net dipole moment. However, there is a non-zero chiral current propagating unidirectionally clockwise (for $Q_T = 1$) or counterclockwise (for $Q_T = -1$) within the A-sublattice unit cell. Such currents for the neighboring cells cancel out each other. However, there will be an uncompensated chiral current at the edge of the 2d plasmonic lattice, which is illustrated in Fig. 6 (e). The corresponding local fields resemble a field of a plasmon polariton propagating clockwise along the edge despite the absence of the edge states, similar to the edge plasmon polaritons in Ref. [32].

There is the second E' mode of the same frequency, which is related to the above-discussed right-rotating one by the application of either \mathcal{T} or σ'_v symmetry operations. That mode is generated in the \mathbf{K}' -valley; it is rotating counter-clockwise within the unit cell and propagating counter-clockwise along the edge. The choice of which one of these modes will be generated is random and is a spontaneous violation of the \mathcal{T} and σ'_v symmetries.

In conclusion, we propose a topological spaser constituted by a honeycomb lattice of spherical metal nanoshells containing a gain medium. The two sublattices, A and B, are built from two different types of nanoshells. Such a spaser generates one of two chiral plasmonic modes characterized by topological charge $Q_T = \pm 1$ whose local fields rotate clockwise or counter-clockwise, respectively. Which of these two modes is generated is determined by a spontaneous violation of symmetry as defined by the initial conditions. The chirality of the spasing mode is stable and topologically protected. The macroscopic fields of the spasing mode are localized along the edge of the lattice despite the absence of the edge states. These edge fields propagate clockwise (for $Q_T = 1$) or counter-clockwise ($Q_T = -1$). Due to a very high lattice momentum $\mathbf{k} = \mathbf{K}$ or $\mathbf{k} = \mathbf{K}'$, they are dark in contrast to the original lasing spaser of Ref. [7]. Nevertheless, they can be outcoupled by using a corresponding coupler, e.g., grating. Application-wise, such a topological spaser is a symmetric bistable that can be used for ultrafast optical storage and processing of information.

Acknowledgments

Major funding was provided by Grant No. DE-FG02-11ER46789 from the Materials Sciences and Engineering Division of the Office of the Basic Energy Sciences, Office of Science, U.S. Department of Energy. Numerical simulations have been performed using support by Grant No. DE-FG02-01ER15213 from the Chemical Sciences, Biosciences and Geosciences Division, Office of Basic Energy Sciences, Office of Science, US Department of Energy. The work of V.A. was supported by NSF EFRI NewLAW Grant EFMA-17 41691. Support for J.W. came from a MURI Grant No. N00014-17-1-2588 from the Office of Naval Research (ONR).

Appendix A: Dipole Modes of metallic spherical shell

The surface plasmon eigenmodes of the i th nanoshell are described by the equation

$$\nabla \left[\theta^{(i)}(\mathbf{r}) \nabla \varphi_m^{(i)} \right] = s_m^{(i)} \nabla^2 \varphi_m^{(i)}. \quad (\text{A1})$$

Function $\theta^{(i)}(\mathbf{r})$ of the nanoshell is equal to 1 inside the metal of the i th nanoshell and 0 elsewhere. The $m = \pm 1$ dipole eigenmode is given by

$$\varphi = \sin \theta e^{im\phi} \begin{cases} c_1 \frac{r}{R_1}, & 0 < r < R_1, \\ c_2 \frac{r}{R_1} + c_3 \frac{R_1^2}{r^2}, & R_1 < r < R_2, \\ c_4 \frac{R_1^2}{r^2}, & R_2 < r. \end{cases} \quad (\text{A2})$$

One finds the eigenvalue $s_m^{(i)}$ for these eigenmodes as

$$s_m^{(i)} = \frac{1 \pm \frac{1}{3} \sqrt{1 + 8\eta^3}}{2}, \quad (\text{A3})$$

where

$$\eta = \frac{R_1}{R_2}. \quad (\text{A4})$$

We impose a normalization condition

$$\int_{\text{All Space}} |\nabla \varphi_m^{(i)}|^2 dv = 1. \quad (\text{A5})$$

There are two solutions corresponding to the \pm signs in Eq. (A3). We choose one corresponding to the $-$ sign, which describes a lower frequency mode. Substituting it, we find:

$$c_1 = \left[\frac{3}{16\pi R_1} \frac{(1 - s_m^{(i)})(s_m^{(i)} - \frac{1}{3})}{(s_m^{(i)} - \frac{1}{2})} \right]^{1/2} = \left[\frac{-1 + 4\eta^3 + \sqrt{1 + 8\eta^3}}{16\pi R_1 \sqrt{1 + 8\eta^3}} \right]^{1/2}, \quad (\text{A6})$$

$$c_2 = \left(\frac{s_m^{(i)} - \frac{2}{3}}{s_m^{(i)} - 1} \right) c_1, \quad (\text{A7})$$

$$c_3 = \frac{1}{3} \left(\frac{-1}{s_m^{(i)} - 1} \right) c_1, \quad (\text{A8})$$

$$c_4 = \frac{1}{3} \left(\frac{-1}{s_m^{(i)} - \frac{1}{3}} \right) c_1. \quad (\text{A9})$$

The electric field of the SP mode inside the gain core, i.e., for $r \leq R_1$, is

$$\begin{aligned} \mathbf{E} &= -A \frac{c_1 e^{im\phi}}{R_1} (\mathbf{e}_r \sin \theta + \mathbf{e}_\theta \cos \theta + i\mathbf{e}_\phi) \\ &= -A \frac{c_1}{R_1} (\mathbf{e}_x + im\mathbf{e}_y), \end{aligned} \quad (\text{A10})$$

where $\mathbf{e}_r, \mathbf{e}_\theta, \mathbf{e}_\phi$ and $\mathbf{e}_x, \mathbf{e}_y$ are the corresponding spherical and Cartesian unit vectors, and

$$A = \sqrt{\frac{4\pi \hbar s_m^{(i)}}{\epsilon_h s_m^{(i)'}}}. \quad (\text{A11})$$

Appendix B: SPP of Plasmonic Array

Consider the problem of two media with permittivities ϵ_d and ϵ_m . The eigenmodes of SP's in the quasistatic limit can be obtained from

$$\nabla [\theta(\mathbf{r})\nabla\varphi] = s\nabla^2\varphi, \quad (\text{B1})$$

with $s = \epsilon_d/(\epsilon_d - \epsilon_m)$ and $\theta(\mathbf{r})$ is 1 inside metal and zero elsewhere. The geometric properties of the eigenmodes are characterized by a generalized eigenvalue problem,

$$\nabla [\theta(\mathbf{r})\nabla\varphi_n] = s_n\nabla^2\varphi_n, \quad (\text{B2})$$

where s_n and φ_n are the eigenvalues and eigenfunctions, respectively. The conditions on the boundary S are

$$\varphi_n \cdot \mathbf{n}\nabla\varphi_n = 0, \quad (\text{B3})$$

where \mathbf{n} is the normal vector to S . Multiplying Eq. (B2) by φ_n and integrating by parts, we obtain

$$s_n = \langle n|\theta(\mathbf{r})|n\rangle, \quad (\text{B4})$$

$$|n\rangle = \nabla\varphi_n, \quad (\text{B5})$$

$$\langle m|n\rangle = \int d^3r (\nabla\varphi_m^*)(\nabla\varphi_n), \quad (\text{B6})$$

The eigenvectors are orthogonal and normalized as,

$$\langle m|n\rangle = \delta_{mn}. \quad (\text{B7})$$

Consider that there are N metal particles (same metal).

$$\nabla [\theta(\mathbf{r})\nabla\varphi_n] = s_n\nabla^2\varphi_n, \quad (\text{B8})$$

$$\theta(\mathbf{r}) = \sum_{i=1}^N \theta^{(i)}(\mathbf{r}). \quad (\text{B9})$$

We can solve Eq. (B8) in terms of the local basis $\varphi_m^{(i)}$, defined as

$$\nabla [\theta^{(i)}(\mathbf{r})\nabla\varphi_m^{(i)}] = s_m^{(i)}\nabla^2\varphi_m^{(i)}, \quad (\text{B10})$$

where $\varphi_m^{(i)}$ are the eigenmodes of the i th metal particle. We expand the total field φ_n in the local basis

$$\varphi_n = \sum_{i,m} C_{nm}^{(i)}\varphi_m^{(i)}, \quad (\text{B11})$$

where $C_{nm}^{(i)}$ are the coefficients to be determined. Substituting Eq. (B11) in Eq. (B8) and using Eq. (B10) we obtained

$$\sum_j \sum_{i \neq j, m} C_{nm}^{(i)} \nabla [\theta_j(\mathbf{r})\nabla\varphi_m^{(i)}] + \sum_{i,m} s_m^{(i)} C_{nm}^{(i)} \nabla^2\varphi_m^{(i)} = s_n \sum_{i,m} C_{nm}^{(i)} \nabla^2\varphi_m^{(i)}, \quad (\text{B12})$$

where the first term describes the inter-particle interaction. To deal with the first term, we expand the field $\nabla\varphi_m^{(i)}$ over the other local eigenstates $\nabla\varphi_{m'}^{(j)}$ ($i \neq j$). The field $\nabla\varphi_m^{(i)}$ inside the j th particle can be expanded over the local basis $\nabla\varphi_{m'}^{(j)}$, since the local basis $\nabla\varphi_{m'}^{(j)}$ forms a complete set of field inside the j th metal.

$$\nabla\varphi_m^{(i)} = \sum_{m'} \beta_{ijmm'} \nabla\varphi_{m'}^{(j)}. \quad (\text{B13})$$

The interaction can be written as

$$\sum_{j,m'} \sum_{i \neq j, m} C_{nm}^{(i)} \beta_{ijmm'} \nabla [\theta_j(\mathbf{r})\nabla\varphi_{m'}^{(j)}] \quad (\text{B14})$$

or equivalently

$$\sum_{j,m'} \sum_{i \neq j, m} C_{nm}^{(i)} \beta_{ijmm'} s_{m'}^{(j)} \nabla^2\varphi_{m'}^{(j)}. \quad (\text{B15})$$

The eigenmode equation becomes

$$\sum_{j,m'} \sum_{i \neq j, m} C_{nm}^{(i)} \beta_{ijmm'} s_{m'}^{(j)} \nabla^2\varphi_{m'}^{(j)} + \sum_{i,m} s_m^{(i)} C_{nm}^{(i)} \nabla^2\varphi_m^{(i)} = s_n \sum_{i,m} C_{nm}^{(i)} \nabla^2\varphi_m^{(i)}. \quad (\text{B16})$$

Multiplying $\varphi_m^{(j)}$ on the both sides, integrating by parts and utilizing the orthogonality of the eigenmodes, we obtain

$$\sum_{i \neq k, m'} C_{nm}^{(i)} \beta_{ikm'm} s_m^{(k)} = (s_n - s_m^{(k)}) C_{nm}^{(k)} \quad (\text{B17})$$

More compactly,

$$\sum_{i,m'} \beta_{ikm'm} s_m^{(k)} C_{nm'}^{(i)} = s_n C_{nm}^{(k)}. \quad (\text{B18})$$

Equation (B18) defines an eigenproblem, which yields the eigenvalue s_n and the coefficients $C_{nm}^{(k)}$. The Hermiticity

of $\beta_{ijmm'}$, i.e.,

$$\beta_{ijmm'} = \beta_{jim'm} \quad (\text{B19})$$

is protected by the Green's reciprocity. The interaction coefficients $\beta_{ijmm'}$ are given by an integral

$$\beta_{ijmm'} = \frac{1}{s_{m'}^{(j)}} \int \theta^{(j)}(\mathbf{r}) \left(\nabla \varphi_{m'}^{(j)*} \right) \left(\nabla \varphi_m^{(i)} \right) d^3r = \frac{1}{s_m^{(i)}} \int \theta^{(i)}(\mathbf{r}) \left(\nabla \varphi_{m'}^{(j)*} \right) \left(\nabla \varphi_m^{(i)} \right) d^3r \quad (\text{B20})$$

$$= \int_{\text{All Space}} \left(\nabla \varphi_{m'}^{(j)*} \right) \left(\nabla \varphi_m^{(i)} \right) d^3r. \quad (\text{B21})$$

Because matrix $\beta_{ikm'm} s_m^{(k)}$ in Eq. (B18) is not Hermitian, the eigenvectors are not orthogonal, and the normalization condition is not $\sum_{i,m} |C_{nm}^{(i)}|^2 = 1$. In actuality, the normalization condition is given by

$$\sum_{i,k,m',m} C_{nm}^{(k)*} \beta_{ikm'm} C_{nm'}^{(i)} = 1. \quad (\text{B22})$$

We can convert Eq. (B18) into a Hermitian eigenproblem by a substitution, $\tilde{C}_{nm}^{(i)} = \sqrt{s_m^{(i)}} C_{nm}^{(i)}$. With this substitution, we rewrite Eq. (B18) as

$$\sum_{i,m'} H_{ikm'm} \tilde{C}_{nm'}^{(i)} = s_n \tilde{C}_{nm}^{(k)}, \quad (\text{B23})$$

$$H_{ikm'm} = \sqrt{s_m^{(i)} s_{m'}^{(j)}} \beta_{ikm'm}. \quad (\text{B24})$$

Because $H_{ikm'm}$ is Hermitian, the eigenvectors are orthogonal and the normalization is simply

$$\sum_{i,m} |\tilde{C}_{nm}^{(i)}|^2 = 1. \quad (\text{B25})$$

Appendix C: Characters of Topological SP Eigenmodes as Irreducible Representations of the D_{3h} Point Symmetry Group

The spasing eigenmodes are surface plasmons (SPs) that should be classified corresponding to irreducible representations of the point symmetry group of the lattice unit cell, which is D_{3h} [31]. This group has six such representations: four of them are singlet or one-dimensional (1d), which are A_1' (scalar or fully-symmetric), A_2' (a pseudovector in the z -direction), A_1'' (pseudoscalar), and A_2'' (a polar vector in the z -direction), and two are doublet or 2d-representations: E' (a polar vector in the xy -plane) and E'' (a pseudovector in the xy -plane). We seek for a solution where the local electric field is in the plane of the lattice (the xy -plane) and rotates in time for a

E	σ_h	$3C_3$	$3S_3$	$3U_2$	$3\sigma'_v$
E'	2	2	-1	-1	0
				0	0

TABLE I: Characters of the E' representation of the D_{3h} point symmetry group, adapted from Ref. 31. The elements of D_{3h} are the identity E , the horizontal-plane reflection σ_h , the three rotations C_3 , the three rotary-reflections S_3 , the three rotations about the horizontal axes U_2 , and the three vertical-plane reflections σ'_v .

given lattice site and in space from a site to a site. A basis for such a field can be constituted, e.g., by two spherical harmonics, $Y_{1\pm 1}$ corresponding to left- and right-handed rotations.

An example of the local fields of the two eigenmodes, which are mutually time-reversed and should be described by the same doublet representation, is provided by our solution of the spaser equations – see the main text of the article. Here we show such two modes: the \mathbf{K} -mode rotating right [Fig. 6] and the \mathcal{T} -reversed \mathbf{K}' -mode rotating left [Fig. 7].

To unambiguously identify the corresponding representation, we note that the underlying material system is a sublattice A whose unit cell has the third-order vertical (z) axis ($3C_3$ symmetry elements), three second-order axes (in the xy plane) ($3U_2$ symmetries), also $3S_3$ elements (mirror-rotational symmetries), and $3\sigma'_v$ elements (reflections in the vertical planes). Spherical harmonics $Y_{1\pm 1}$ are spherical representations of a polar vector in the xy plane:

$$Y_{1\pm 1} = \mp \frac{1}{2} \sqrt{\frac{3}{2\pi}} (x \pm iy). \quad (\text{C1})$$

The character of the trivial E operation is always the representation dimensionality, i.e., $\chi(E) = 2$. To find $\chi(\sigma_h)$ for our eigenvectors we note that the σ_h operation is reflection in the xy mirror plane (i.e., a transformation $x \rightarrow x$, $y \rightarrow y$, and $z \rightarrow -z$), which leaves both of the basis functions of Eq. (C1) unchanged. Correspondingly, $\chi(\sigma_h) = 2$. Operation C_3 is a rotation

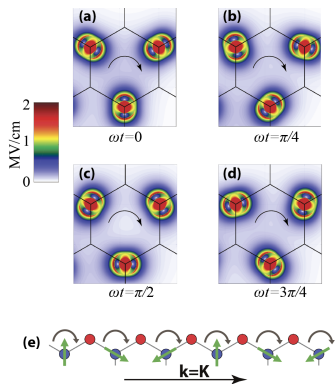


FIG. 6: Dynamics of \mathbf{K} -valley SP eigenmode. (a)-(d) The distributions of the local field modulus are plotted for the unit cell in the real space. The phases of the spaser oscillation are indicated for each panel. The color-coded scale of the local fields is given at the left=hand side for one SP quantum per the unit supercell. The local fields rotate in time in the direction of the black arrow, i.e., clockwise. (e) Edge fields for \mathbf{K} -valley mode. The instantaneous dipole vectors are indicated by the green arrows; the direction of the field rotation is depicted by the curved black arrows; crystal momentum \mathbf{k} of the mode is shown by the straight black arrow. Each such a rotating dipole generates a current that is normal to this dipole.

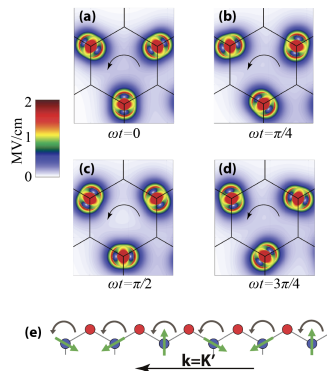


FIG. 7: Dynamics of the \mathbf{K}' -valley SP eigenmode. Same as Fig. 6 but the dynamics is \mathcal{T} -reversed: fields rotate left and propagate left.

by a $2\pi/3$ angle whose character, obviously, is $\chi(C_3) = 2 \cos(2\pi/3) = -1$. An operation S_3 is a product of σ_h , which leaves the basis unchanged, and C_3 ; thus its character is $\chi(S_3) = \chi(C_3) = -1$. A U_2 rotation, say about the y axis of symmetry, causes $y \rightarrow y, x \rightarrow -x$; this results in $Y_{11} \leftrightarrow Y_{1-1}$. Thus the basis functions are exchanged, and the corresponding transformation matrix is purely off-diagonal; correspondingly, $\chi(U_2) = 0$. An operation σ'_v acts for our purposes exactly like U_2 ; thus $\chi(\sigma'_v) = 0$. These characters that we have obtained are exactly those of the E' representation of the D_{3h} group summarized in Table I. This unambiguously identifies that our spasing eigenmodes transform accordingly to the E' doublet representation of the D_{3h} point symmetry group. Note that that the two components of this doublet describe field distribution rotating in time and space in the opposite directions. They transform one into another by either of the following transformations: \mathcal{T} , σ'_v , or U_2 .

-
- [1] D. J. Bergman and M. I. Stockman, Surface plasmon amplification by stimulated emission of radiation: Quantum generation of coherent surface plasmons in nanosystems, *Phys. Rev. Lett.* **90**, 027402 (2003).
- [2] M. I. Stockman and D. J. Bergman, Surface plasmon amplification by stimulated emission of radiation (spaser), US Patent 7,569,188 (2009).
- [3] M. I. Stockman, The spaser as a nanoscale quantum generator and ultrafast amplifier, *Journal of Optics* **12**, 024004 (2010).
- [4] K. Li, X. Li, M. I. Stockman, and D. J. Bergman, Surface plasmon amplification by stimulated emission in nanolenses, *Phys. Rev. B* **71**, 115409 (2005).
- [5] D. Y. Fedyanin, Toward an electrically pumped spaser, *Opt. Lett.* **37**, 404 (2012).
- [6] D. G. Baranov, A. P. Vinogradov, A. A. Lisyansky, Y. M. Strel'niker, and D. J. Bergman, Magneto-optical spaser, *Opt. Lett.* **38**, 2002 (2013).
- [7] N. I. Zheludev, S. L. Prosvirnin, N. Papisimakis, and V. A. Fedotov, Lasing spaser, *Nat. Phot.* **2**, 351 (2008).
- [8] M. A. Noginov, G. Zhu, A. M. Belgrave, R. Bakker, V. M. Shalaev, E. E. Narimanov, S. Stout, E. Herz, T. Suteewong, and U. Wiesner, Demonstration of a spaser-based nanolaser, *Nature* **460**, 1110 (2009).
- [9] R. F. Oulton, V. J. Sorger, T. Zentgraf, R.-M. Ma, C. Gladden, L. Dai, G. Bartal, and X. Zhang, Plas-

- mon lasers at deep subwavelength scale, *Nature* **461**, 629 (2009).
- [10] R.-M. Ma, R. F. Oulton, V. J. Sorger, G. Bartal, and X. Zhang, Room-temperature sub-diffraction-limited plasmon laser by total internal reflection, *Nat. Mater.* **10**, 110 (2010).
- [11] R. A. Flynn, C. S. Kim, I. Vurgaftman, M. Kim, J. R. Meyer, A. J. Mäkinen, K. Bussmann, L. Cheng, F. S. Choa, and J. P. Long, A room-temperature semiconductor spaser operating near 1.5 micron, *Opt. Express* **19**, 8954 (2011).
- [12] M. J. H. Marell, B. Smalbrugge, E. J. Geluk, P. J. van Veldhoven, B. Barcones, B. Koopmans, R. Nötzel, M. K. Smit, and M. T. Hill, Plasmonic distributed feedback lasers at telecommunications wavelengths, *Opt. Express* **19**, 15109 (2011).
- [13] F. v. Beijnum, P. J. v. Veldhoven, E. J. Geluk, M. J. A. d. Dood, G. W. t. Hooft, and M. P. v. Exter, Surface plasmon lasing observed in metal hole arrays, *Phys. Rev. Lett.* **110**, 206802 (2013).
- [14] Y.-J. Lu, C.-Y. Wang, J. Kim, H.-Y. Chen, M.-Y. Lu, Y.-C. Chen, W.-H. Chang, L.-J. Chen, M. I. Stockman, C.-K. Shih, and S. Gwo, All-color plasmonic nanolasers with ultralow thresholds: Autotuning mechanism for single-mode lasing, *Nano Lett.* **14**, 43814388 (2014).
- [15] Q. Zhang, G. Li, X. Liu, F. Qian, Y. Li, T. C. Sum, C. M. Lieber, and Q. Xiong, A room temperature low-threshold ultraviolet plasmonic nanolaser, *Nat. Commun.* **5**, 4953 (2014).
- [16] B. T. Chou, Y. H. Chou, Y. M. Wu, Y. C. Chung, W. J. Hsueh, S. W. Lin, T. C. Lu, T. R. Lin, and S. D. Lin, Single-crystalline aluminum film for ultraviolet plasmonic nanolasers, *Sci. Rep.* **6**, 19887 (2016).
- [17] C.-J. Lee, H. Yeh, F. Cheng, P.-H. Su, T.-H. Her, Y.-C. Chen, C.-Y. Wang, S. Gwo, S. R. Bank, C.-K. Shih, and W.-H. Chang, Low-threshold plasmonic lasers on a single-crystalline epitaxial silver platform at telecom wavelength, *ACS Photonics* **4**, 1431 (2017).
- [18] S. Sun, C. Zhang, K. Wang, S. Wang, S. Xiao, and Q. Song, Lead halide perovskite nanoribbon based uniform nanolaser array on plasmonic grating, *ACS Photonics* **4**, 649656 (2017).
- [19] R.-M. Ma, S. Ota, Y. Li, S. Yang, and X. Zhang, Explosives detection in a lasing plasmon nanocavity, *Nature Nanotechnology* **9**, 600 (2014).
- [20] S. Wang, B. Li, X. Y. Wang, H. Z. Chen, Y. L. Wang, X. W. Zhang, L. Dai, and R. M. Ma, High-yield plasmonic nanolasers with superior stability for sensing in aqueous solution, *ACS Photonics* **4**, 1355 (2017).
- [21] X. Y. Wang, Y. L. Wang, S. Wang, B. Li, X. W. Zhang, L. Dai, and R. M. Ma, Lasing enhanced surface plasmon resonance sensing, *Nanophotonics* **6**, 472 (2017).
- [22] E. I. Galanzha, R. Weingold, D. A. Nedosekin, M. Sarimollaoglu, J. Nolan, W. Harrington, A. S. Kuchyanov, R. G. Parkhomenko, F. Watanabe, Z. Nima, A. S. Biris, A. I. Plekhanov, M. I. Stockman, and V. P. Zharov, Spaser as a biological probe, *Nat. Commun.* **8**, 15528 (2017).
- [23] W. Zhou, M. Dridi, J. Y. Suh, C. H. Kim, D. T. Co, M. R. Wasielewski, G. C. Schatz, and T. W. Odom, Lasing action in strongly coupled plasmonic nanocavity arrays, *Nature Nano* **8**, 506 (2013).
- [24] M. I. Stockman, Lasing spaser in two-dimensional plasmonic crystals, *NPG Asia Mater.* **5**, e71 (2013).
- [25] M. V. Berry, Quantal phase factors accompanying adiabatic changes, *Proc. Royal Soc. London Ser. A* **392**, 45 (1984).
- [26] D. Xiao, M.-C. Chang, and Q. Niu, Berry phase effects on electronic properties, *Reviews of Modern Physics* **82**, 1959 (2010).
- [27] R. Guo, M. Necada, T. K. Hakala, A. I. Vakevainen, and P. Torma, Lasing at k points of a honeycomb plasmonic lattice, *Phys. Rev. Lett.* **122**, 013901 (2019).
- [28] Y. M. You, X. X. Zhang, T. C. Berkelbach, M. S. Hybertsen, D. R. Reichman, and T. F. Heinz, Observation of biexcitons in monolayer wse_2 , *Nat. Phys.* **11**, 477 (2015).
- [29] K. S. Novoselov, A. Mishchenko, A. Carvalho, and A. H. C. Neto, 2d materials and van der Waals heterostructures, *Science* **353**, 461 (2016).
- [30] D. N. Basov, M. M. Fogler, and F. J. G. de Abajo, Polaritons in van der waals materials, *Science* **354**, aag1992 (2016).
- [31] L. D. Landau and E. M. Lifshitz, *Quantum Mechanics: Non-Relativistic Theory* (Pergamon Press, Oxford and New York, 1965).
- [32] J. C. W. Song and M. S. Rudner, Chiral plasmons without magnetic field, *Proceedings of the National Academy of Sciences* **113**, 4658 (2016).
- [33] D. J. Bergman and D. Stroud, Properties of macroscopically inhomogeneous media, in *Solid State Physics*, Vol. 46, edited by H. Ehrenreich and D. Turnbull (Academic Press, Boston, 1992) pp. 148–270.
- [34] M. I. Stockman, S. V. Faleev, and D. J. Bergman, Localization versus delocalization of surface plasmons in nanosystems: Can one state have both characteristics?, *Phys. Rev. Lett.* **87**, 167401 (2001).
- [35] P. B. Johnson and R. W. Christy, Optical constants of noble metals, *Phys. Rev. B* **6**, 4370 (1972).